

Systematics of leading particle production

F. O. Durães*

*Instituto de Física, Universidade de São Paulo, C.P. 66318, 05315-970 São Paulo, SP, Brazil*F. S. Navarra[†]*Instituto de Física, Universidade de São Paulo, C.P. 66318, 05315-970 São Paulo, SP, Brazil
and Soltan Institute for Nuclear Studies, Nuclear Theory Department ul. Hoża 69, 00-681 Warsaw, Poland*G. Wilk[‡]*Soltan Institute for Nuclear Studies, Nuclear Theory Department ul. Hoża 69, 00-681 Warsaw, Poland*

(Received 24 April 1998; published 6 October 1998)

Using a QCD-inspired model developed by our group for particle production, the interacting gluon model (IGM), we have made a systematic analysis of all available data on leading particle spectra. These data include diffractive collisions and photoproduction at DESY HERA. With a small number of parameters (essentially only the nonperturbative gluon-gluon cross section and the fraction of diffractive events) good agreement with data is found. We show that the difference between pion and proton leading spectra is due to their different gluon distributions. We predict a universality in the diffractive leading particle spectra in the large momentum region, which turns out to be independent of the incident energy and of the projectile type. [S0556-2821(98)08121-1]

PACS number(s): 13.85.Ni, 12.39.Ki

I. INTRODUCTION

In high energy hadron-hadron collisions the momentum spectra of outgoing particles which have the same quantum number as the incoming particles, also called leading particle (LP) spectra, have been measured already some time ago [1]. Recently new data on pion-proton collisions were released by the EHS/NA22 Collaboration [2] in which the spectra of both outgoing leading particles, the pion and the proton, were simultaneously measured. Very recently data on leading protons produced in electron-proton reactions at the DESY *ep* collider HERA with a c.m. system (c.m.s.) energy one order of magnitude higher than in the other above-mentioned hadronic experiments became available [3]. In the case of photoproduction data can be interpreted in terms of the vector dominance model [4] and can therefore be considered as data on LP production in vector meson-proton collisions. These new measurements of LP spectra both in hadron-hadron and in electron-proton collisions have renewed interest in the subject, especially because the latter are measured at higher energies and therefore the energy dependence of the LP spectra can now be determined.

It is important to have a very good understanding of these spectra for a number of reasons. They are the input for calculations of the LP spectra in hadron-nucleus collisions, which are a fundamental tool in the description of atmospheric cascades initiated by cosmic radiation [5]. There are several new projects in cosmic ray physics including the High Resolution Fly's Eye Project, the Telescope Array Project, and the Pierre Auger Project [6] for which a precise

knowledge of energy flow (LP spectra and inelasticity distributions) in very high energy collisions would be very useful.

In a very different scenario, namely, in high energy heavy ion collisions at the BNL Relativistic Heavy Ion Collider (RHIC), it is very important to know where the outgoing (leading) baryons are located in momentum space. If the stopping is large, they will stay in the central rapidity region and affect the dynamics there, generating, for example, a baryon-rich equation of state. Alternatively, if they populate the fragmentation region, the central (and presumably hot and dense) region will be dominated by mesonic degrees of freedom. The composition of the dense matter is therefore relevant for the study of quark gluon plasma formation [7].

In any case, before modelling *p-A* or *A-A* collisions one has to understand properly hadron-hadron processes. The LP spectra are also interesting for the study of diffractive reactions, which dominate the large x_F region.

Since LP spectra are measured in reactions with low momentum transfer and go up to large x_F values, it is clear that the processes in question occur in the nonperturbative domain of QCD. One needs then "QCD-inspired" models and the most popular are string models, such as FRITIOF, VENUS, or the quark gluon string model (QGSM). Calculations of LP spectra involving these models can be found in Refs. [8] and [9].

In the framework of the QCD parton model of high energy collisions, leading particles originate from the emerging fast partons of the collision debris. There is a large rapidity separation between fast partons and sea partons. Fast partons interact rarely with the surrounding wee partons. The interaction between the hadron projectile and the target is primarily through wee parton clouds. A fast parton or a coherent configuration of fast partons may therefore filter through essentially unaltered. Based on these observations and aiming to study *p-A* collisions, the authors of Ref. [8] proposed a

*Email address: fduraes@if.usp.br

[†]Email address: navarra@if.usp.br[‡]Email address: Grzegorz.Wilk@fuw.edu.pl

mechanism for LP production in which the LP spectrum is given by the convolution of the parton momentum distribution in the projectile hadron with its corresponding fragmentation function into a final leading hadron. This independent fragmentation scheme is, however, not supported by leading charm production in pion-nucleus scattering. It fails especially in describing the D^-/D^+ asymmetry. A number of models addressed these data and the conclusion was that valence quark recombination is needed. Translated to leading pion or proton production this means that what happens is rather a coalescence of valence quarks to form the LP and not an independent fragmentation of a quark or diquark to a pion or a nucleon. Another point is that the coherent configuration formed by the valence quarks may go through the target but, due to the strong stopping of the gluon clouds, may be significantly decelerated. This correlation between central energy deposition due to gluons and leading particle spectra was shown to be essential for the understanding of leading charm production [10].

In this work we follow the same general ideas of Ref. [8] but with a different implementation. In particular we replace independent fragmentation by valence quark recombination and free leading parton flow by deceleration due to ‘‘gluon stripping.’’ These ideas are incorporated in the model employed by us, the interacting gluon model (IGM), which has been used to study energy flow in nondiffractive reactions [11,12] and has been recently extended to diffractive processes [13] and also applied to the recent HERA (photoproduction) data both on diffractive mass distributions [14] and leading J/ψ spectra [15].

We shall study all measured LP spectra including those measured at HERA. We will find and comment on universal aspects in the energy flow pattern of all these reactions. Universality means, in the context of the IGM, that the underlying dynamics is the same both in diffractive and nondiffractive LP production and both in hadron-hadron and photon-hadron processes.

II. INTERACTING GLUON MODEL

The interacting gluon model was introduced some time ago [11], developed by us recently [12,13], and proved to be quite useful for the study of energy flow. Since the model has been extensively discussed in our previous papers, we shall present here only the basic ideas and a few formulas, leaving the more detailed discussion to the Appendix. The main aspect of the IGM, shared with minijet models such as HIJING [16], is the assumption that hadron-hadron reactions are dominated by multiple and incoherent parton-parton scatterings. Among these, gluon-gluon scatterings are the most important. At very high energies and large scales this is a very good approximation. At not very large energies and lower scales one is already moving towards the nonperturbative domain and dealing with soft gluons and the incoherence hypothesis might not be valid.

The soft gluons involved in the collisions studied here are partly preexisting inside the hadron and partly produced by radiation. Preexisting soft gluons exhibit the same properties as those studied in lattice QCD simulations in the strong

coupling regime. According to di Giacomo and Panagopoulos [17], the typical correlation length of the soft gluon fields is around 0.2–0.3 fm. Since this length is still much smaller than the typical hadron size, the gluon fields can, in a first approximation, be treated as uncorrelated. As a consequence [18] the number of (soft) gluon-gluon collisions will follow a Poissonian distribution, which was also used in Refs. [16,19,20]. In the case of radiated soft gluons, it was recently shown in [21] that gluons produced with small transverse momenta are independently emitted from the radiating parton, as QCD coherence suppresses their showering. Consequently, the multiplicity of low p_T gluons follows a Poisson distribution, suggesting that the collision number follows a Poisson distribution as well. These facts indicate that in the region where perturbative results break down, the independent collision approximation may still be a reasonable one. From the practical point of view, it was shown in [11] that replacing the Poissonian distribution by a broader one does not affect the results significantly as long as some mass scale is introduced to cut off the very low x region.

In the IGM the two colliding hadrons are represented by valence quarks carrying their quantum numbers (charges) plus the accompanying clouds of gluons (which represent also the sea $q\bar{q}$ pairs and therefore should be regarded as effective gluons). In the course of a collision gluonic clouds interact strongly and form a gluonic *central fireball* (CF) located in the central region of the reaction. The valence quarks (plus those gluons which did not interact) get excited and form *leading jets* (LJ’s) (or *beam jets*) which then populate mainly the fragmentation regions of the reaction.

The valence quarks are therefore spectators and the bulk of the reaction and energy deposition occurs because of the gluon-gluon collisions, whose number is Poisson distributed with the mean value given by

$$\frac{d\bar{n}}{dx' dy'} = \omega(x', y') = \frac{\sigma_{gg}(x' y' s)}{\sigma(s)} \times G(x') G(y') \Theta(x' y' - K_{min}^2), \quad (1)$$

where G ’s denote the effective number of gluons from the corresponding projectiles (approximated by the respective gluonic structure functions) and σ_{gg} and σ are the gluon-gluon and hadron-hadron cross sections, respectively. In the above expression x' and y' are the fractional momenta of two gluons coming from the projectile and from the target whereas $K_{min} = m_0/\sqrt{s}$ (with m_0 being the mass of lightest produced state and \sqrt{s} the total c.m.s. energy). Each gluon-gluon collision produces a minifireball (MF). Depending on the energy many g - g collisions may happen and energy fractions $x = \sum_i n_i x'_i$ and $y = \sum_i n_i y'_i$ from the target and projectile may be deposited in the central region. The probability for depositing the energy fractions x and y can be analytically computed in the IGM and is given by the function $\chi(x, y)$ derived in the Appendix.

Leading particles can also be diffractively produced. In the IGM diffractive dissociation (DD) can be included in a simple way, by just requiring that one of the colliding had-

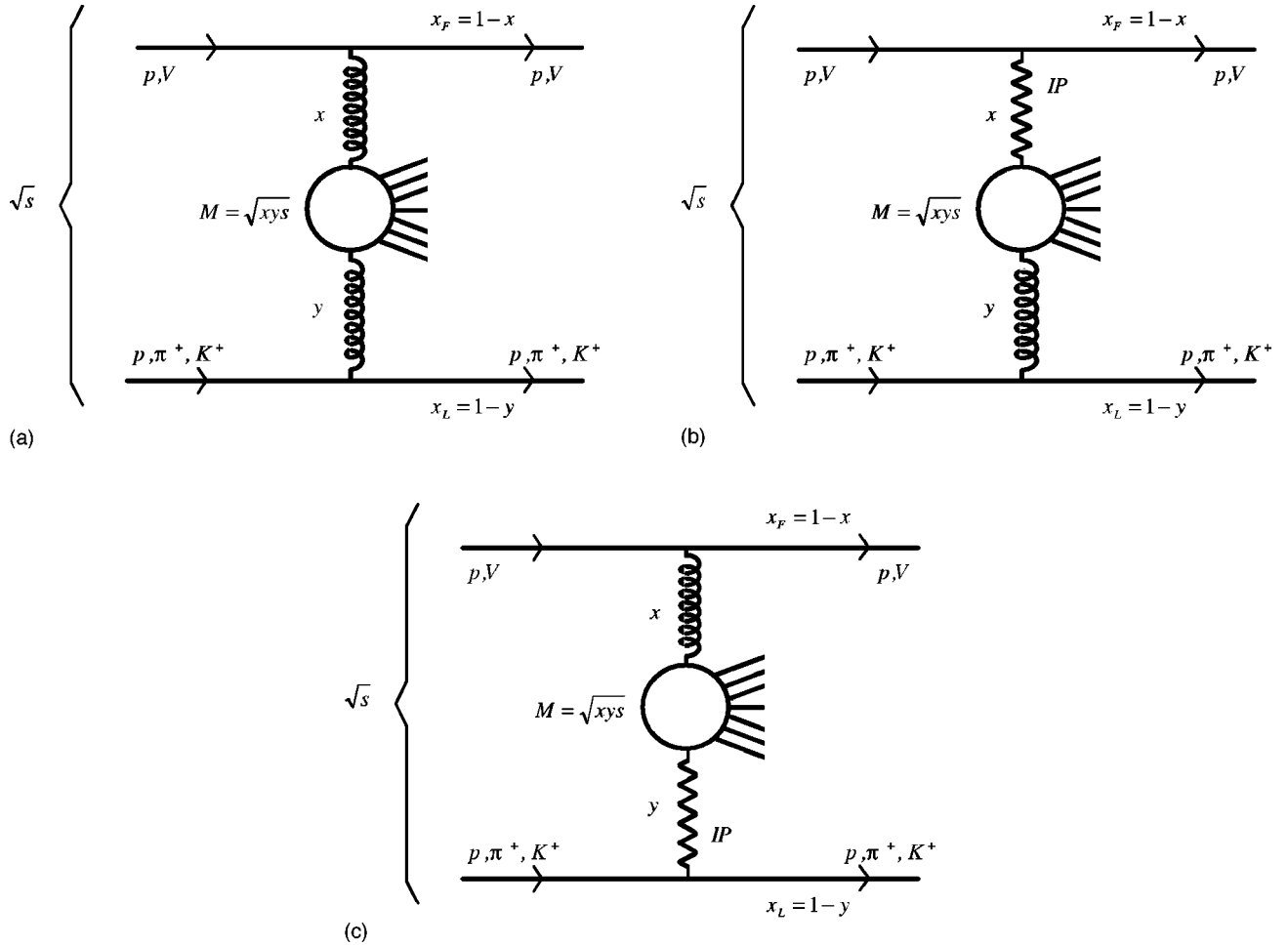


FIG. 1. A schematic description of the IGM. (a) we show a nondiffractive event. The upper (lower) leg represents the leading particle with the momentum fraction $x_F = 1 - x$ ($x_L = 1 - y$). In (b) the hadron in the upper leg sends a P with momentum fraction x and remains a leading particle with momentum fraction $x_F = 1 - x$. (c) corresponds to the case where P is emitted from a hadron in the lower leg, which keeps momentum $x_L = 1 - y$.

rons loses only a very small fraction of its initial energy momentum. This was done by imposing cuts on the first moments of the ω function [13]. In our earlier calculations of energy flow with the IGM we were not concerned with the fragmentation region. The main interest was the energy deposition in the central region, which is highly relevant for quark gluon plasma physics. Therefore our first LP spectra were in reasonable agreement with data but in the region $x_L \geq 0.8$ the model prediction was below the experimental points because we had no diffractive component whereas the data did not discriminate between diffractive and nondiffractive events. Later on we have included diffraction in the IGM [13]. The resulting picture is the same as for nondiffractive events, except that in DD the gluon cloud of the projectile interacts only with a subset of the target gluon cloud, which carries a small momentum fraction and which we call ‘‘Pomeron’’ (P). Our Pomeron is essentially just a kinematical restriction which forces one of the colliding hadrons to lose only a very small amount of its energy. Using the diffractive IGM we have obtained a good description of the diffractive mass spectra in hadronic diffractive collisions [13] and also in photon-proton collisions [14]. Although it is

possible to reformulate the model in the impact parameter space and associate diffractive events with peripheral collisions, as done in Ref. [22], we prefer here to explore further the kinematical interpretation of diffraction. Moreover, in the present formulation we correctly reproduce the diffractive peak, which was not obtained in Ref. [22]. Apart from the recent EHS/NA22 and HERA LP spectra, a new experiment now under consideration at Fermilab will, among other things, address the question of leading particles and DD component in the near future [23]. In view of these facts we shall recalculate LP spectra in our model with a DD component properly included and extend it to $e-p$ collisions.

III. LEADING HADRON SPECTRA

In the IGM a typical nondiffractive event is shown in Fig. 1(a). Colliding particles lose energy fractions x and y , forming leading particles with $x_F = 1 - x$ and $x_L = 1 - y$. In the figure, V stands for vector meson, used later for photoproduction at HERA. We shall consider the reactions $p + p \rightarrow p + X$, $\pi^+ + p \rightarrow \pi^+ + X$, $K^+ + p \rightarrow K^+ + X$, and $\pi^+ + p \rightarrow \pi^+ + p + X$. Later we also address photon-proton reac-

tions in the VDM approach: $p + V \rightarrow p + X$. Diffractive processes are illustrated in Figs. 1(b) and 1(c), where the Pomeron is emitted from the target and from the projectile respectively. In Figs. 1(a), 1(b), and 1(c) the probability to form a CF with mass $M = \sqrt{xy}s$ is called $\chi^{nd}(x,y)$, $\chi_1^d(x,y)$, and $\chi_2^d(x,y)$, respectively. These functions were derived in our earlier works (cf., for example, [13]).

With the functions $\chi(x,y)$ we obtain the corresponding LP spectra just by changing variables and by adding the resulting distributions with proper weights.

In the lower legs of Fig. 1, leading particles emerge from the collision keeping momentum fraction x_L with distribution $F_{LP}(x_L)$ given by

$$\begin{aligned}
 F_{LP}(x_L) &= \int_0^1 dx \int_0^1 dy \left[(1-\alpha) \chi^{nd}(x,y) \right. \\
 &\quad \left. + \sum_{j=1,2} \alpha_j \chi_j^d(x,y) \right] \delta(x_L - 1 + y) \\
 &\quad \times \Theta \left(xy - \frac{m_0^2}{s} \right) \Theta \left[y - \frac{(M_{LP} + m_0)^2}{s} \right] \\
 &= (1-\alpha) \int_{x_{min}}^1 dx \chi^{(nd)}(x; y=1-x_L) \\
 &\quad + \sum_{j=1,2} \alpha_j \int_{x_{min}}^1 dx \chi_j^{(d)}(x; y=1-x_L), \quad (2)
 \end{aligned}$$

where α is the total fraction of diffractive events and α_1 and α_2 are the fractions of diffractive events with a Pomeron emitted from the upper and lower legs in Fig. 1, respectively. They satisfy the condition $\alpha_1 + \alpha_2 = \alpha$. In the above expression M_{LP} and m_0 denote the mass of the LP and the mass of the lightest CF produced and the limits of integration are defined by

$$x_{min} = \text{Max} \left[\frac{m_0^2}{(1-x_L)s}, \frac{(M_{LP} + m_0)^2}{s} \right]. \quad (3)$$

The main physical quantities in Eq. (2) are the functions (cf. the Appendix for details of derivation and justification)

$$\begin{aligned}
 \chi^{nd}(x,y) &= \frac{\chi_0^{nd}}{2\pi\sqrt{D_{xy}}} \exp \left\{ -\frac{1}{2D_{xy}} [\langle y^2 \rangle (x - \langle x \rangle)^2 \right. \\
 &\quad \left. + \langle x^2 \rangle (y - \langle y \rangle)^2 \right. \\
 &\quad \left. - 2\langle xy \rangle (x - \langle x \rangle)(y - \langle y \rangle)] \right\}, \quad (4)
 \end{aligned}$$

with

$$D_{xy} = \langle x^2 \rangle \langle y^2 \rangle - \langle xy \rangle^2, \quad (5)$$

$$\langle x^n y^m \rangle = \int_0^1 dx' x'^n \int_0^1 dy' y'^m \omega^{nd}(x', y'), \quad (6)$$

and

$$\begin{aligned}
 \chi_j^d(x,y) &= \frac{\chi_{j0}^d}{2\pi\sqrt{D_{xy}^{(j)}}} \exp \left\{ -\frac{1}{2D_{xy}^{(j)}} [\langle y_j^2 \rangle (x - \langle x_j \rangle)^2 \right. \\
 &\quad \left. + \langle x_j^2 \rangle (y - \langle y_j \rangle)^2 \right. \\
 &\quad \left. - 2\langle x_j y_j \rangle (x - \langle x_j \rangle)(y - \langle y_j \rangle)] \right\}, \quad (7)
 \end{aligned}$$

with

$$D_{xy}^{(j)} = \langle x_j^2 \rangle \langle y_j^2 \rangle - \langle x_j y_j \rangle^2, \quad (8)$$

$$\langle x_j^n y_j^m \rangle = \int_0^{x_{max}^{(j)}} dx' x'^n \int_0^{y_{max}^{(j)}} dy' y'^m \omega^d(x', y'). \quad (9)$$

The index values of $j=1$ and $j=2$ correspond to the diagrams in Figs. 1(b) and 1(c), respectively. Here $y_{max}^{(1)} = 1$, $y_{max}^{(2)} = y$, $x_{max}^{(1)} = x$, and $x_{max}^{(2)} = 1$ and χ_0^{nd} and χ_{j0}^d are the proper normalization factors assuring that $\int_0^1 dx_L F_{LP}(x_L) = 1$. We separately normalize to unity both components entering Eq. (2). This procedure is crucial in our case in order to assure the proper overall energy-momentum conservation, which is a characteristic feature of any implementation of the IGM.

The weight α is essentially our new parameter. It should be of the order of the ratio between the total diffractive and total inelastic (including DD processes) cross sections, $\sigma_{tot}^{diff}/\sigma_{tot}^{inel}$. It can, however, differ from that ratio due to the different experimental acceptance of DD and non-DD events not considered here. This fact makes α a free parameter of the model. We assume it to be independent of the total c.m.s. energy. Indeed the fraction of diffractive events with respect to the total number of events or the ratio between diffractive and total inelastic cross sections are quantities which depend weakly on the c.m.s. energy of the collision. They may depend more strongly on detector coverage and acceptance. The reactions that we discuss here occur at c.m.s. energies ranging from 14 up to 100 GeV. This is still a relatively moderate variation in the energy. Since we do not address diffraction at the SppS (energies of 200 – 900 GeV) or at the Tevatron (energy of 1800 GeV), we keep our fraction of diffractive events as a constant. This quantity is the only free parameter in this paper.

The spectral functions ω^{nd} and ω^d are the same as in [12] and [13,14] for nondiffractive and for diffractive processes, respectively. We refer the reader to [12–14] for details concerning the exact values and character of the relevant parameters which were fixed from other previous applications of the IGM. In the case of diffractive hadron-proton scattering the function $G(y)$ in Eq. (1) represents the momentum dis-

tribution of the gluons belonging to the proton subset called Pomeron and y is the momentum fraction of the proton carried by one of these gluons. We shall therefore use the notation $G(y) = G_P(y)$. This function should not be confused with the momentum distribution of the gluons inside the Pomeron, $f_{g/P}(\beta)$ (see below).

The moments $\langle q^n \rangle$, $q = x, y$ (we only require $n = 1, 2$), are the only places where dynamical quantities like the gluonic and hadronic cross sections appear in the IGM. In DD we are selecting a special class of events and therefore we must choose the correct dynamical inputs in the present situation, namely, $G_P(y)$ and the hadronic cross section σ appearing in ω^d .

As already mentioned, the Pomeron for us is just a collection of gluons which form a color singlet and belong to the diffracted hadron. In early works we have assumed that these gluons behave like all other ordinary gluons in the proton and have therefore the same momentum distribution. The only difference is the momentum sum rule, which for the gluons in P is

$$\int_0^1 dy y G_P(y) = p, \quad (10)$$

where $p \approx 0.05$ (see [13] and below) instead of $p \approx 0.5$, which holds for the entire gluon population in the proton.

In principle, since the Pomeron can not be considered an ordinary particle, one cannot define precisely a momentum sum rule in the usual sense [24,25]. Nevertheless, in our definition, the Pomeron is really just a collection of gluons. As such, when emitted, it carries a momentum fraction p of the parent proton. Of course, p can fluctuate. In the calculations, it always appears divided by the Pomeron-proton cross section, which is another poorly known and fluctuating quantity. Taking all these fluctuations into account would just introduce more freedom in the model and make calculations more complicated. We avoid it in this paper as we also avoid other sources of fluctuations such as impact parameter fluctuations. In Ref. [22] impact parameter fluctuations were introduced in the nondiffractive IGM and the result was, as expected, a smearing of the original curves. The overall effect, however, was not very big. We expect the same to be true for the fluctuations in the Pomeron sum rule.

In [14] we have treated the Pomeron structure in more detail and addressed the question of its ‘‘hardness’’ or ‘‘softness.’’ In order to make contact with the analysis performed by HERA experimental groups we have considered two possible momentum distributions for the gluons inside P , one hard, $f_{g/P}^h(\beta)$, and the other soft, $f_{g/P}^s(\beta)$. Following the (standard) notation of Ref. [26], β is the momentum fraction of the Pomeron carried by the gluons and the superscripts h and s denote hard and soft, respectively. Using a standard choice for the Pomeron, flux factor, $f_{P/p}(x_P)$, where x_P is the fraction of the proton momentum carried by the Pomeron, and noticing that $\beta = x/x_P$, the distribution $G_P(y)$ needed in Eq. (1) is then given by the convolution

$$G_P^{h,s}(y) = \int_y^1 \frac{dx_P}{x_P} f_{P/p}(x_P) f_{g/P}^{h,s}\left(\frac{y}{x_P}\right). \quad (11)$$

In Ref. [14] we have also used $G_P(y) = 6(1-y)^5/y$, the same expression already used by us before in Ref. [13]. As was shown, this choice corresponds to an intermediate structure between ‘‘soft’’ and ‘‘hard’’ Pomeron and it shall be used here.

One of the most interesting conclusions of Ref. [14] was that it is possible to learn something about the Pomeron profile studying the diffractive mass spectra. Moreover, our analysis suggests that the ‘‘soft’’ Pomeron is in conflict with these data. Only with a very unusual choice of parameters could a good agreement be recovered. Considering the large amount of data already described previously by the IGM, this choice was extreme and we concluded therefore that the ‘‘soft’’ Pomeron is disfavored. The same conclusion was found in Refs. [26,27]. The fraction of diffracted nucleon momentum, p , allocated specifically to the P gluonic cluster and the hadronic cross section σ are both unknown. However, they always appear in ω as a ratio (p/σ) of parameters and different choices are possible. Just in order to make use of the present knowledge about the Pomeron, we shall choose

$$\sigma(s) = \sigma^{Pp} = a + b \ln \frac{s}{s_0}, \quad (12)$$

where $s_0 = 1 \text{ GeV}^2$ and $a = 2.6 \text{ mb}$ and $b = 0.01 \text{ mb}$ are parameters fixed from our previous [13] systematic data analysis. As can be seen, $\sigma(s)$ turns out to be a very slowly varying function of \sqrt{s} assuming values between 2.6 and 3.0 mb, which is a well accepted value for the Pomeron-proton cross section, and $p \approx 0.05$ (cf. [13]).

As will be seen, a good understanding of the systematics of LP production can be obtained in terms of the dynamical inputs contained in Eq. (1). With the exception of α all parameters are fixed. In the next section we compare our results given by Eq. (2) with experimental data.

IV. RESULTS AND DISCUSSION

In Figs. 2(a), 2(b), and 2(c) we present our spectra of leading protons, pions, and kaons, respectively. The dashed lines show the contribution of nondiffractive LP production and the solid lines show the effect of adding a nondiffractive component. All parameters were fixed previously and the only one to be fixed was α . For simplicity we have neglected the second diagram in Fig. 1, because it gives a curve which is very similar in shape to the nondiffractive curve. In contrast, the Pomeron emission by the projectile [Fig. 1(c)] produces the diffractive peak. We have then chosen $\alpha_1 = 0$ and $\alpha_2 = \alpha = 0.3$ in all collision types. As expected, the inclusion of the diffractive component flattens considerably the final LP distribution, bringing it to a good agreement with the available experimental data [1]. In our model there is some room for changes, leading to fits with better quality. We could, for example, use a prescription for hadronization (as we did before in [12]) giving a more important role to it, as done in Ref. [8]. In doing this, however, we lose simplicity and the transparency of the physical picture, which are the advantages of the IGM. We prefer to keep simplicity and

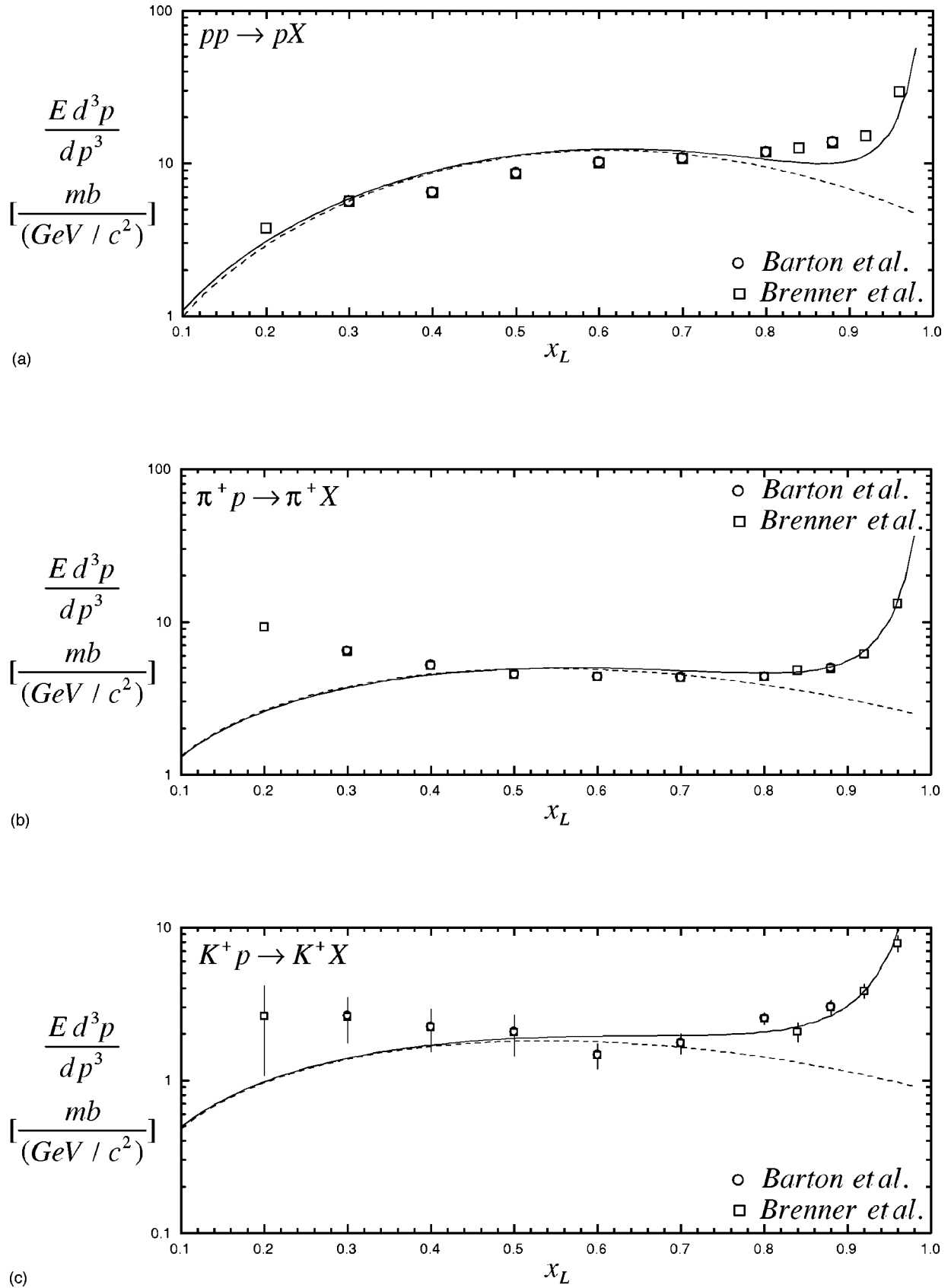


FIG. 2. Comparison of our spectra $F(x_L)$ with data from Ref. [1] for (a) leading protons, (b) leading pions, and (c) leading kaons. Dashed and solid lines show the nondiffractive component and the total curve respectively.

concentrate on the interpretation of our results. In first place it is interesting to observe the good agreement between our curve and data for protons [Fig. 1(a)] in the low x region. The observed protons could have been also centrally produced; i.e., they could come from the CF. However, we fit data without the CF contribution. This suggests, as expected, that all the protons in this x range are leading; i.e., they come from valence quark recombination. In Figs. 1(b) and 1(c) we observe an excess at low x . This is so because pions and kaons are light and they can more easily be created from the sea (centrally produced). Our distributions come only from the leading jet (LJ) and consequently pass below the data points. A closer look at the three dashed lines in Fig. 1 shows that pion and kaon spectra are softer than the proton one. The former peak at $x \approx 0.56$ while the latter peaks at $x \approx 0.62$. In the IGM this can be understood as follows. The energy fraction that goes to the central fireball, $K = \sqrt{xy}$, is controlled by the behavior of the function $\chi(x, y)^{nd}$, which is approximately a double Gaussian in the variables x and y , as can be seen in expression (4). The quantities $\langle x \rangle$ and $\langle y \rangle$ play the role of central values of this Gaussian. Consequently, when $\langle x \rangle$ or $\langle y \rangle$ increases, this means that the energy deposition from the upper or lower leg (in Fig. 1) increases, respectively. The quantities $\langle x \rangle$ and $\langle y \rangle$ are the moments of the ω function and are directly proportional to the gluon distribution functions in the projectile and target and inversely proportional to the target-projectile inelastic cross section. In the calculations, there are two changes when we go from p - p to π - p .

(i) The first is that we replace σ_{inel}^{pp} by $\sigma_{inel}^{\pi p}$ which is smaller. This leads to an overall increase of the energy deposition. There are some indications that this is really the case and the inelasticity in π - p is larger than in p - p collisions [28].

(ii) The second and most interesting and important change is that we replace the one gluon distribution in the proton $G^p(y)$ by the corresponding distribution in the pion $G^\pi(y)$. We know that $G^p(y) \approx (1-y)^5/y$ whereas $G^\pi(y) \approx (1-y)^2/y$, i.e., that gluons in pions are harder than in protons. This introduces an asymmetry in the moments $\langle x \rangle$ and $\langle y \rangle$, making the latter significantly larger.

As a consequence, pions will be more stopped and will emerge from the collision with a softer x spectrum. This can already be seen in the data points of Fig. 2. However, since these points contain particles produced by other mechanisms, such as central and diffractive production, it is not yet possible to draw firm conclusions.

The analysis of the moments $\langle x \rangle$ and $\langle y \rangle$ can also be done for the diffractive process shown in Fig. 1(c). Because of the cuts in the integrations in Eq. (9), they will depend on $x_L = 1-y$. We calculate them for $p+p \rightarrow p+X$ and $\pi+p \rightarrow \pi+X$ reactions. For low x_L they assume very similar values as in the nondiffractive case. For large x_L , however, we find that $\langle x \rangle_p \approx \langle x \rangle_\pi$ and $\langle y \rangle_p \approx \langle y \rangle_\pi$. The reason for these approximate equalities is that in diffractive processes we cut the large y' region and this is precisely where the pion and the proton would differ, since only for large y are $G_p^p(y) \approx (1-y)^5/y$ and $G_p^\pi(y) \approx (1-y)^2/y$ significantly different.

In Ref. [13] we have shown that the introduction of the above-mentioned cuts drastically reduces the energy (\sqrt{s}) dependence of the diffractive mass distributions, leading, in particular, to the approximate $1/M_x^2$ behavior for all values of \sqrt{s} from ISR to Tevatron energies. Here these cuts produce another type of scaling, which may be called ‘‘projectile scaling’’ or ‘‘projectile universality of the diffractive peak’’ and which means that for large enough x_L the diffractive peak is the same for all projectiles. The corresponding χ^d functions will be the same for protons and pions in this region. The cross section appearing in the denominator of the moments will, in this case, be the same, i.e., σ^{pp} . The only remaining difference between them, their different gluonic distributions, is in this region cutoff. This may be regarded as a prediction of the IGM. Experimentally this may be difficult to check since one would need a large number of points in large x_L region of the leading particle spectrum. Data plotted in Fig. 2 neither prove nor disprove this conjecture. The discrepancy observed in the proton spectrum is only due to our choice of normalization of the diffractive and nondiffractive curves. The peak shapes are similar.

The EHS/NA22 Collaboration provided us with data on $\pi^+ + p \rightarrow \pi^+ + p + X$ reactions. In particular they present the x distributions of both leading particles, the pion and the proton. Their points for pions and protons are shown in Figs. 3(a) and 3(b), respectively. These points are presumably free from diffractive dissociation. The above-mentioned asymmetry in pion and proton energy loss emerges clearly, the pions being much slower. The proton distribution peaks at $x_F \approx 0.6-0.8$. Our curves (solid lines) reproduce with no free parameter this behavior and we obtain a good agreement with the pion spectrum. Proton data show an excess at large x_F that we are not able to reproduce keeping the same values of parameters as before.

The authors of Ref. [2] tried to fit their measured proton spectrum with the FRITIOF code and could not obtain a good description of data. This indicates that these large x points are a problem for standard multiparticle production models as well. In our case, if we change our parameter m_0 from the usual value $m_0 = 0.35$ GeV to $m_0 = 0.45$ GeV, we can reproduce most of data points both for pions and protons as well. This is not a big change and indicates that the model would be able to accommodate this new experimental information. Of course, a definite statement about the subject would require a global refitting procedure, which is not our main concern now.

If, at high energies, the reactions p - p and π - p have the same characteristics and if the vector dominance model (VDM) is good hypothesis (as it seems to be), then more about the energy flow in meson- p collisions can be learned at HERA. Indeed, as mentioned in [14], at the HERA electron-proton collider the bulk of the cross section corresponds to photoproduction, in which a beam electron is scattered through a very small angle and a quasireal photon interacts with the proton. For such small virtualities the dominant interaction mechanism takes place via fluctuation of the photon into a hadronic state which interacts with the proton via the strong force [4]. High energy photoproduction exhibits there-

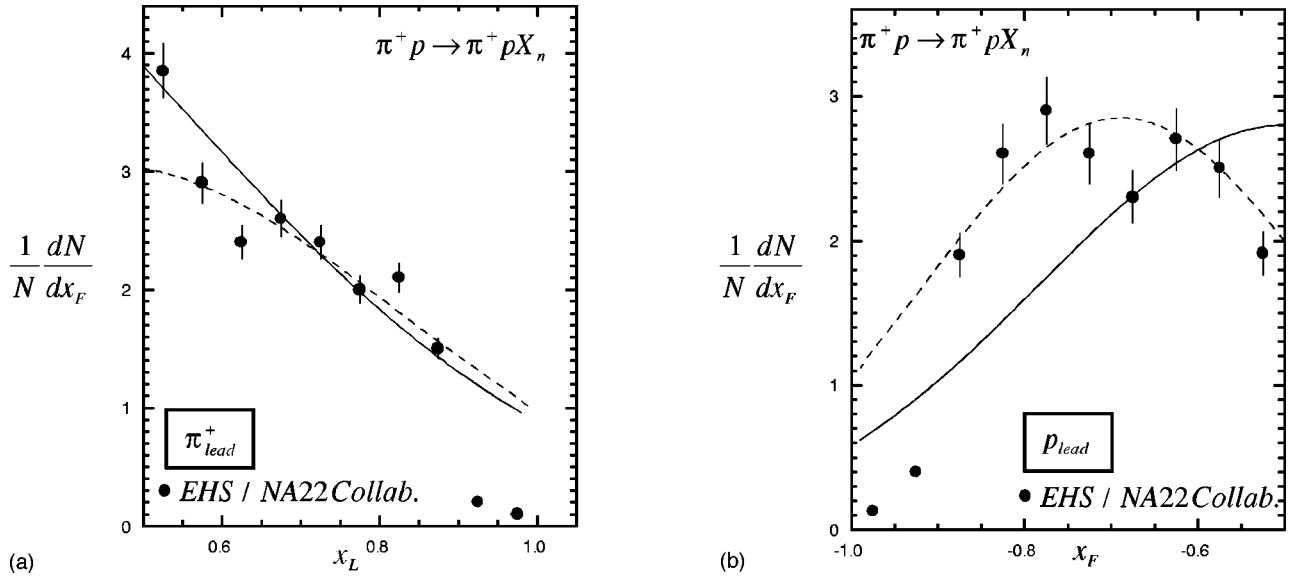


FIG. 3. (a) Comparison of our spectra $F(x_L)$ for leading pions with data from Ref. [2] in the reaction $\pi^+ + p \rightarrow \pi^+ + p + X$. Solid and dashed lines correspond to the choices $m_0 = 0.35$ GeV and $m_0 = 0.45$ GeV, respectively. (b) the same as (a) for the leading proton spectrum $F(x_F)$ measured in the same reaction.

fore similar characteristics to hadron-hadron interactions. Recent data taken by the ZEUS Collaboration at HERA [3] show that the LP spectra measured in photoproduction and in deep inelastic scattering (DIS) (where $Q^2 \geq 4$ GeV²) are very similar, specially in the large x_L region. This suggests that, as pointed out in [29], the QCD hardness scale for particle production in DIS gradually decreases from a (large) Q^2 , which is relevant in the photon fragmentation region, to a soft scale in the proton fragmentation region, which is the one considered here. We can therefore expect a similarity of the inclusive spectra of the leading protons in high energy hadron-proton collisions, discussed above, and in virtual photon-proton collisions. In other words, we may say that the photon is neither resolving nor being resolved by the fast emerging protons. This implies that these reactions are dominated by some nonperturbative mechanism. This is confirmed by the failure of perturbative QCD [30] (implemented by the Monte Carlo codes ARIADNE and HERWIG) when applied to the proton fragmentation region. In Ref. [29] the LP spectra were studied in the context of meson and Pomeron exchanges. Here we use the vector meson dominance hypothesis and describe leading proton production in the same way as done for hadron-hadron collisions. The only change is that now we have ρ - p instead of p - p collisions. Whereas this may be generally true for photoproduction, it remains an approximation for DIS, valid in the large x_L region.

In Fig. 1 we show schematically the IGM picture of a photon-proton collision. According to it, during the interaction the photon is converted into a hadronic (mesonic) state and then interacts with the incoming proton. This hadronic state is called V in the upper legs of Figs. 1(a), 1(b), and 1(c). At HERA only V - p collisions are relevant. The meson-proton interaction follows then the usual IGM picture; namely, the valence quarks fly through essentially undisturbed whereas the gluonic clouds of both projectiles interact strongly with each other. The state V loses a fraction x of its

original momentum and gets excited carrying a $x_F = 1 - x$ fraction of the initial momentum. The proton, which we shall call here the diffracted proton, loses only a fraction y of its momentum but otherwise remains intact. We shall assume here, for simplicity, that the vector meson is a ρ^0 and take $G^{\rho^0}(x) = G^\pi(x)$ in Eq. (1). In Fig. 4 we compare our results with ZEUS data. The agreement is again good.

V. CONCLUSIONS

We have analyzed leading particle spectra in terms of the IGM, which includes now also a contribution coming from the diffractive processes. The new component improved dramatically the agreement with all existing data on hadron-hadron collisions.

As long as the energy flow is concerned the IGM works extremely well with essentially two parameters: the nonperturbative gluon-gluon cross section and the fraction of diffractive events. This should enlarge considerably its range of applicability in analyses of cosmic ray data.

At the same time, assuming the VDM, we were able to describe equally well the leading proton spectra in e - p reactions. Also here the inclusion of a diffractive component provided by the new version of the IGM turns out to be crucial to get good agreement with data.

We have shown that the difference between pion and proton leading spectra is due to their different gluon distributions [31]. We predict a universality in the diffractive leading particle spectra in the large momentum region, which turns out to be independent of the incident energy and of the projectile type.

ACKNOWLEDGMENTS

This work has been supported by FAPESP, under contract 95/4635-0, CNPQ (Brazil), and KBN (Poland). F.S.N. would

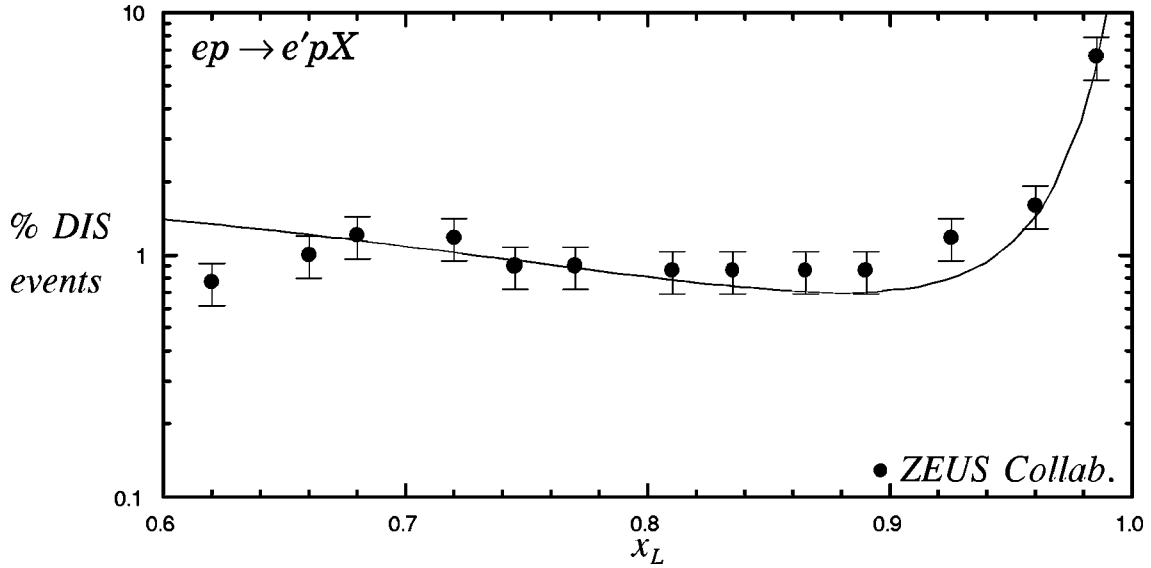


FIG. 4. Comparison between our calculation and the LP spectrum measured at HERA by the ZEUS Collaboration [3].

also like to thank the The Andrzej Soltan Institute for Nuclear Studies, Warsaw, for the warm hospitality extended to him during his visit there. We would like to thank Dr. E.C. de Oliveira and Dr. Z. Włodarczyk for helpful discussions on diffractive and cosmic ray experiments.

APPENDIX

We shall collect together here the main points concerning the interacting gluon model scattered throughout the literature [10–15]. The IGM is based on the idea that since about half of a hadron momentum is carried by gluons, and since gluons interact more strongly than quarks, during a collision there is a separation of constituents. Valence quarks tend to be fast forming leading particles whereas gluons tend to be stopped in the central rapidity region. It belongs therefore to the class of models exploring the concept of partons and of hard and semihard collisions (like those presented by Gaisser and Stanev [19], Sjostrand and van Zijl [20], Wang and Gyulassy [16], or Geiger [32]). The latter are collisions between partons at a moderate scale [$Q^2 \approx (2 \text{ GeV})^2$], which, however, still allows for the use of perturbative QCD. The scattered partons form the so-called minijets. At $\sqrt{s} = 540 \text{ GeV}$ the minijet cross section is already 25% of the total inelastic cross section. However, apart from some ambiguity in choosing the semihard scale, these models have to face the problem that even at very high energies a significant part of a hadronic collision occurs at scales lower than the semihard one. The attitude taken in HUIJING [16], in the parton cascade model [32], and also in the IGM is to extrapolate these quantities to lower scales. These extrapolations can be continuously improved, especially in view of the advance of our knowledge on nonperturbative effects. There are, for example, models for distribution functions which work at scales as low as 0.3 GeV^2 [33]. As for σ one can compute nonperturbative effects in the context of an operator product expansion. In spite of these limitations these models have the advantage of dealing with partons and being thus prepared to

incorporate perturbative QCD in a natural way. This is welcome since perturbative processes are expected to be increasingly important at higher energies. Compared to the other models mentioned above, the IGM is simpler because it is designed to study energy flow and makes no attempt to calculate cross sections or to follow hadronization in great detail. This simplifies the calculations and avoids time-consuming numerical simulations. The most important aspect of the IGM, shared with those models, is the assumption of multiple parton-parton incoherent scattering which is implicit in the Poissonian distribution of the number of parton-parton collisions (which is also used in Refs. [20,19,16]) used below.

The IGM is therefore based on the assumed dominance of hadronic collisions by gluonic interactions and can be summarized in the following way.

(i) The two colliding hadrons are represented by valence quarks carrying their quantum numbers (charges) plus the accompanying clouds of gluons (which represent also the sea $q\bar{q}$ pairs and therefore should be regarded as effective ones).

(ii) In the course of a collision the gluonic clouds interact strongly, depositing in the central region of the reaction fractions x and y of the initial energy-momenta of the respective projectiles in the form of a gluonic *central fireball*.

(iii) The valence quarks (plus those gluons which did not interact) get excited and form *leading jets*, which then populate mainly the fragmentation regions of the reaction.

The fraction of energy stored in the CF is therefore equal to $K = \sqrt{x \cdot y}$ and its rapidity is $Y = \frac{1}{2} \ln(x/y)$. These two quantities provide then a sort of dynamically calculated initial conditions for any statistical model of multiparticle production and that was one of the initial aims of the IGM.

According to the IGM the CF consists of *minifireballs* formed from pairs of colliding gluons. In collisions at higher scales a MF is the same as a pair of minijets or jets. In the study of energy flow the details of fragmentation and hadron production are not important. Most of the MF's will be in the

central region and we assume that they coalesce, forming the CF. The collisions leading to MF's occur at different energy scales given by $Q_i^2 = x_i y_i s$, where the index i labels a particular kinematic configuration where the gluon from the projectile has momentum x_i and the gluon from the target has y_i . We have to choose the scale where we start to use perturbative QCD. Many studies in the literature converge to the value $Q_{min}^2 = p_{T min}^2 = (2.3 \text{ GeV})^2$. Below this value we have to assume that we can still talk about individual soft gluons, and because of the short correlation length (found in lattice QCD calculations) between them, they still interact mostly pairwise. In this region we can no longer use the distribution functions extracted from DIS or the perturbative elementary cross sections.

The central quantity in the IGM is the probability to form a CF carrying momentum fractions x and y of two colliding hadrons. It is defined as the sum over an undefined number n of MF's:

$$\begin{aligned} \chi(x, y) &= \sum_{n_1} \sum_{n_2} \cdots \sum_{n_i} \delta[x - n_1 x_1 - \cdots - n_i x_i] \\ &\quad \times \delta[y - n_1 y_1 - \cdots - n_i y_i] \cdot P(n_1) \cdots P(n_i) \\ &= \sum_{\{n_i\}} \left\{ \delta\left[x - \sum_i n_i x_i\right] \delta\left[y - \sum_i n_i y_i\right] \right\} \prod_{\{n_i\}} P(n_i). \end{aligned} \quad (\text{A1})$$

The delta functions in the above expression guarantee energy-momentum conservation and $P(n_i)$ is the probability to have n_i collisions between gluons with x_i and y_i . If the collisions are independent, $P(n_i)$ is given by

$$P(n_i) = \frac{(\bar{n}_i)^{n_i} \exp(-\bar{n}_i)}{n_i!}. \quad (\text{A2})$$

Inserting $P(n_i)$ in Eq. (A1) and using the following integral representations for the delta functions,

$$\delta\left[x - \sum_i n_i x_i\right] = \frac{1}{2\pi} \int_{-\infty}^{+\infty} dt \exp\left[it\left(x - \sum_i n_i x_i\right)\right], \quad (\text{A3})$$

$$\delta\left[y - \sum_i n_i y_i\right] = \frac{1}{2\pi} \int_{-\infty}^{+\infty} du \exp\left[iu\left(y - \sum_i n_i y_i\right)\right], \quad (\text{A4})$$

we can perform all summations and products, arriving at

$$\begin{aligned} \chi(x, y) &= \frac{1}{(2\pi)^2} \int_{-\infty}^{+\infty} dt \int_{-\infty}^{+\infty} du \exp[i(tx + uy)] \\ &\quad \times \exp\left\{ \sum_i \bar{n}_i [e^{-i(tx_i + uy_i)} - 1] \right\}. \end{aligned} \quad (\text{A5})$$

Taking now the continuum limit

$$\bar{n}_i = \frac{d\bar{n}_i}{dx' dy'} \Delta x' \Delta y' \rightarrow d\bar{n} = \frac{d\bar{n}}{dx' dy'} dx' dy', \quad (\text{A6})$$

we obtain

$$\begin{aligned} \chi(x, y) &= \frac{1}{(2\pi)^2} \int_{-\infty}^{+\infty} dt \int_{-\infty}^{+\infty} du \exp[i(tx + uy)] \\ &\quad \times \exp\left\{ \int_0^1 dx' \int_0^1 dy' \omega(x', y') \right. \\ &\quad \left. \times [e^{-i(tx' + uy')} - 1] \right\}, \end{aligned} \quad (\text{A7})$$

where

$$\omega(x', y') = \frac{d\bar{n}}{dx' dy'}. \quad (\text{A8})$$

This function $\omega(x', y')$, sometimes called the spectral function, represents the average number of gluon-gluon collisions as a function of x' and y' , contains all the dynamical inputs of the model, and has the form

$$\omega(x', y') = \frac{\sigma_{gg}(x' y' s)}{\sigma(s)} G(x') G(y') \Theta(x' y' - K_{min}^2), \quad (\text{A9})$$

where G 's denote the effective number of gluons from the corresponding projectiles (approximated by the respective gluonic structure functions) and σ_{gg} and σ are the gluon-gluon and hadron-hadron cross sections, respectively. In the above expression x' and y' are the fractional momenta of two gluons coming from the projectile and from the target whereas $K_{min} = m_0/\sqrt{s}$, with m_0 being the mass of lightest produced state and \sqrt{s} the total c.m.s. energy. m_0 is a parameter of the model. The integral in the second line of Eq. (A7) is dominated by the low x' and y' region. Considering the singular behavior of the $G(x)$ distributions at the origin we make the following approximation:

$$[e^{-i(tx' + uy')} - 1] \simeq -i(tx' + uy') - \frac{1}{2}(tx' + uy')^2. \quad (\text{A10})$$

With this approximation it is possible to perform the integrations in Eq. (A7) and obtain the final expression for $\chi(x, y)$ discussed in the main text:

$$\begin{aligned} \chi(x, y) &= \frac{\chi_0}{2\pi\sqrt{D_{xy}}} \exp\left\{ -\frac{1}{2D_{xy}} [\langle y^2 \rangle (x - \langle x \rangle)^2 + \langle x^2 \rangle (y - \langle y \rangle)^2 - 2\langle xy \rangle (x - \langle x \rangle)(y - \langle y \rangle)] \right\}, \end{aligned} \quad (\text{A11})$$

where

$$D_{xy} = \langle x^2 \rangle \langle y^2 \rangle - \langle xy \rangle^2$$

and

$$\langle x^n y^m \rangle = \int_0^1 dx x^n \int_0^1 dy y^m \omega(x, y). \quad (\text{A12})$$

Here χ_0 is a normalization factor defined by the condition

$$\int_0^1 dx \int_0^1 dy \chi(x, y) \theta(xy - K_{min}^2) = 1. \quad (\text{A13})$$

In order to evaluate the distribution (A11) we need to choose the value of m_0 , the semihard scale $p_{T min}$, and define $G(x)$ and σ_{gg} in both interaction regimes. We take $p_{T min} = 2.3$ GeV and $m_0 = 0.35$ GeV. These are the two scales present in the model. The semihard gluon-gluon cross section is taken, at order α_s^2 , to be

$$\hat{\sigma}_{gg}^h(x, y, s) = \kappa \frac{\pi}{16 p_{T min}^2} [\alpha_s(Q^2)]^2 H, \quad (\text{A14})$$

where

$$H = 36T + \frac{51\lambda T}{4xy} - \frac{3\lambda^2 T}{8x^2 y^2} + \frac{9\lambda}{xy} \ln \left[\frac{1-T}{1+T} \right] \quad (\text{A15})$$

and

$$T = \left[1 - \frac{\lambda}{xy} \right]^{1/2}, \quad \lambda = \frac{4 p_{T min}^2}{s}. \quad (\text{A16})$$

The parameter κ is the one frequently used to incorporate higher corrections in α_s and is $1.1 \leq \kappa \leq 2.5$ according to the choice of $G(x)$, of the scale Q^2 and $p_{T min}$. For $p_{T min} = 2.3$ GeV, $\kappa = 2.5$. The coupling constant is given by

$$\alpha_s(Q^2) = \frac{12 \pi}{(33 - 2N_f) \ln \left[\frac{Q^2}{\Lambda^2} \right]}, \quad (\text{A17})$$

where $\Lambda = 0.2$ GeV and $N_f = 3$ is the number of active flavors. As usual in minijet physics we choose $Q^2 = p_{T min}^2$ and use the distributions $G(x, Q^2)$ parametrized in the literature.

When the invariant energy of the gluon pair \hat{s} is the interval $m_0^2 \leq \hat{s} = xy s \leq 4 p_{T min}^2$ we are outside the perturbative domain. Parton-parton cross sections in the nonperturbative regime have been parametrized in [34], leading to a successful quark-gluon model for elastic and diffractive scattering. Recently these nonperturbative cross sections have been calculated in the stochastic vacuum model [35]. The obtained cross sections are functions of the gluon condensate and of the gluon field correlation length, both quantities extracted from lattice QCD calculations. In order to keep our treatment simple we shall adopt the older parametrization for the gluon-gluon cross section used in [34]:

$$\hat{\sigma}_{gg}^s(x, y, s) = \frac{\alpha}{xys} \quad (\text{A18})$$

where α is the second parameter of the model [11].

-
- [1] D.S. Barton *et al.*, Phys. Rev. D **27**, 2580 (1983); A.E. Brenner *et al.*, *ibid.* **26**, 1497 (1982).
- [2] EHS/NA22 Collaboration, N.M. Agababyan *et al.*, Z. Phys. C **75**, 229 (1996).
- [3] N. Cartiglia, ‘‘Leading Baryons at Low x_L in DIS and Photo-production at ZEUS,’’ hep-ph/9706416.
- [4] S.D. Holmes, W. Lee, and J.E. Wiss, Annu. Rev. Nucl. Part. Sci. **35**, 397 (1985); T.H. Bauer, R.D. Spital, D.R. Yennie, and F.M. Pipkin, Rev. Mod. Phys. **50**, 261 (1978).
- [5] G.M. Frichter, T.K. Gaisser, and T. Stanev, Phys. Rev. D **56**, 3135 (1997).
- [6] Cf., for example, A.A. Watson, Nucl. Phys. B (Proc. Suppl.) **60**, 171 (1998); J.W. Cronin, *ibid.* **28**, 213 (1992); ‘‘The Pierre Auger Project,’’ Design Report, 2nd ed., 1996, <http://www-tdauger.fnal.gov:82>.
- [7] Cf., for example, *Quark Matter’ 96*, Proceedings [Nucl. Phys. **A610**, 1 (1996)], and references therein.
- [8] A. Berera *et al.*, Phys. Lett. B **403**, 1 (1997).
- [9] W.D. Walker, Phys. Rev. C **53**, 1886 (1996).
- [10] F.O. Durães, F.S. Navarra, C.A.A. Nunes, and G. Wilk, Phys. Rev. D **53**, 6136 (1996).
- [11] G.N. Fowler, F.S. Navarra, M. Plümer, A. Vourdas, R.M. Weiner, and G. Wilk, Phys. Rev. C **40**, 1219 (1989).
- [12] F.O. Durães, F.S. Navarra, and G. Wilk, Phys. Rev. D **47**, 3049 (1993); **50**, 6804 (1994).
- [13] F.O. Durães, F.S. Navarra, and G. Wilk, Phys. Rev. D **55**, 2708 (1997).
- [14] F.O. Durães, F.S. Navarra, and G. Wilk, Phys. Rev. D **56**, R2499 (1997).
- [15] F.O. Durães, F.S. Navarra, and G. Wilk, ‘‘Leading Particle Effect in J/Ψ Elasticity Distribution,’’ hep-ph/9803325; Mod. Phys. Lett. A (to be published).
- [16] X.N. Wang and M. Gyulassy, Phys. Rev. D **44**, 3501 (1991); **45**, 844 (1992).
- [17] A. di Giacomo and H. Panagopoulos, Phys. Lett. B **285**, 133 (1992).
- [18] N. Brown, Mod. Phys. Lett. A **4**, 2447 (1989).
- [19] T.K. Gaisser and T. Stanev, Phys. Lett. B **219**, 375 (1989).
- [20] T. Sjostrand and M. van Zijl, Phys. Rev. D **36**, 2019 (1987).
- [21] S. Lupia, W. Ochs, and J. Wosiek, ‘‘Poissonian limit of soft gluon multiplicity,’’ hep-ph/9804419.
- [22] S. Paiva, Y. Hama, and T. Kodama, Phys. Rev. C **55**, 1455 (1997); Y. Hama and S. Paiva, Phys. Rev. Lett. **78**, 3070 (1997).
- [23] A. Brandt *et al.*, ‘‘A forward proton detector at D0,’’ Report No. FERMILAB-PUB-97/377, 1997; E. Oliveira (private communication).
- [24] ZEUS Collaboration, M. Derrick *et al.*, Eur. Phys. J. C **5**, 41 (1998).
- [25] R.J.M. Covolan and M.S. Soares, Phys. Rev. D **37**, 180 (1998).

- [26] ZEUS Collaboration, M. Derrick *et al.*, Phys. Lett. B **356**, 129 (1995); Z. Phys. C **68**, 569 (1995), and references therein.
- [27] H1 Collaboration, T. Ahmed *et al.*, Nucl. Phys. **B435**, 3 (1995); **B429**, 477 (1994).
- [28] For example, in the cosmic ray experiments it is usually assumed that $K_{\pi N} = 1.5 K_{pp}$, which is traced to analysis of data like those by G. Donaldson *et al.*, Phys. Lett. **73B**, 375 (1978), performed in terms of the additive quark models [cf. E. Fishbach and G.W. Look, Phys. Rev. D **15**, 2576 (1977)]; Z. Włodarczyk (private communication).
- [29] A. Szczurek, N.N. Nikolaev, and J. Speth, Phys. Lett. B **428**, 383 (1998).
- [30] ZEUS Collaboration, M. Derrick *et al.*, Phys. Lett. B **384**, 388 (1996).
- [31] One should mention here that there is another possible difference between nucleons and mesons which can contribute to the different behavior of the leading particles in both cases. It is connected with the triple gluon junction present (in some models) in baryons but not in mesons, which, if treated as elementary object, can influence substantially LP spectra [cf. D. Kharzeev, Phys. Lett. B **378**, 238 (1996), and references therein]. We shall not discuss this possibility in this paper.
- [32] K. Geiger, Phys. Rev. D **46**, 4965 (1992); **46**, 4986 (1992).
- [33] M. Glück, E. Reya, and A. Vogt, Z. Phys. C **47**, 433 (1995); A. Edin and G. Ingelman, "A model for the parton distributions in hadrons," Report No. TSL/ISV-98-0194, DESY 98-035, hep-ph/9803496.
- [34] P. L'Hereux, B. Margolis, and P. Valin, Phys. Rev. D **32**, 1 (1985).
- [35] A.F. Martini, M.J. Menon, and D.S. Thober, Phys. Rev. D **57**, 3026 (1998).